NIH Public Access
Author Manuscript
J Struct Biol. Author manuscript; available in PMC 2009 November 30.

Published in final edited form as:
J Struct Biol. 2009 October ; 168(1): 168–176. doi:10.1016/j.jsb.2009.02.004.

The M34A mutant of Connexin26 reveals active conductance states in pore-suspending membranes

Oliver Gaßmann[a], **Mohamed Kreir**[b], **Cinzia Ambrosi**[c], **Jennifer Pranskevich**[c], **Atsunori Oshima**[e], **Christian Röling**[a], **Gina Sosinsky**[c,d], **Niels Fertig**[b], and **Claudia Steinem**[a,*]

[a]Institute for Organic and Biomolecular Chemistry, University of Göttingen, Tammannstr. 2, 37077 Göttingen, Germany

[b]Nanion Technologies GmbH, Erzgiessereistr. 4, 80335 München, Germany

[c]National Center for Microscopy and Imaging Research, University of California, San Diego, CA, USA

[d]Department of Neurosciences, University of California, San Diego, CA, USA

[e]Department of Biophysics, Kyoto University, Oiwake, Kitashirakawa, Sakyo-ku, Kyoto 606-8502, Japan

Abstract

Connexin26 (Cx26) is a member of the connexin family, the building blocks for gap junction intercellular channels. These dodecameric assemblies are involved in gap junction-mediated cell-cell communication allowing the passage of ions and small molecules between two neighboring cells. Mutations in Cx26 lead to the disruption of gap junction-mediated intercellular communication with consequences such as hearing loss and skin disorders. We show here that a mutant of Cx26, M34A, forms an active hemichannel in lipid bilayer experiments. A comparison with the Cx26 wild-type is presented. Two different techniques using micro/nano-structured substrates for the formation of pore-suspending lipid membranes are used. We reconstituted the Cx26 wild-type and Cx26M34A into artificial lipid bilayers and observed single channel activity for each technique, with conductance levels of around 35, 70 and 165 pS for the wildtype. The conductance levels of Cx26M34A were found at around 45 and 70 pS.

Keywords

Connexon; Gap junction; GUV; Nano-BLM; Planar lipid bilayer; Single channel recordings

1. Introduction

Connexins (Cx) are members of a multigene family of membrane-spanning proteins that form intercellular channels, which are composed of two hexameric hemichannels, called connexons. These intercellular channels organize into gap junctional plaques and span the extracellular space/matrix of adjacent cells, thus allowing a passive exchange of small molecules up to about 1 kDa (Harris, 2001).

© 2009 Elsevier Inc. All rights reserved.

*Corresponding author. Fax: +49 551 39 3228. claudia.steinem@chemie.uni-goettingen.de (C. Steinem).

NIH-PA Author Manuscript
NIH-PA Author Manuscript
NIH-PA Author Manuscript

NIH-PA Author Manuscript

NIH-PA Author Manuscript

NIH-PA Author Manuscript

Cx26 and Cx30 are two major isoforms highly expressed in the cochlear supporting cells and fibrocytes (Ahmad et al., 2003; Forge et al., 2003; Kikuchi et al., 1995; Lautermann et al., 1999). The supporting cells in the organ of Corti are massively coupled by gap junctions. They are believed to remove potassium ions from the hair cells during auditory transduction (Gerido and White, 2004; Jentsch, 2000) and recycle them back to the endolymph (Kikuchi et al., 2000). Mutations in this system can cause deafness by disrupting this intercellular ionic movement and disrupting homeostasis. Eventually, this breakdown in homeostasis leads to cell death in the supporting cells upon repeated tonic stimulation. In this context, some Cx26 mutants have been reported to decrease or even nullify the gap junction conductance between supporting cells (Zhang et al., 2005).

M34T is a deafness-related Cx26 mutant that can cause prelingual nonsyndromic hereditary deafness (Kelsell et al., 1997). An analogous mutant, M34A, has been used for electron crystallographic analysis. Structure determination of Cx26M34A 2D-crystals revealed a plug-like density at the cytoplasmic mouth of the pore (Oshima et al., 2007), which is drastically reduced in case of an *N*-terminal deletion mutant Cx26M34Adel2-7 (Oshima et al., 2008). In addition, various *N*-terminal deletion constructs still allow for oligomerization, cell surface expression and docking of two hemichannels, but electrical coupling is eliminated (Kyle et al., 2008). Taken together with the site specific mutagenesis performed by Verselis and colleagues (Purnick et al., 2000; Oh et al., 2000), this suggests that the *N*-terminus of connexins play an essential role in the gating of gap junction channels. Other studies propose the importance of methionine at position 34 for channel functionality and regulation. Experiments with transiently transfected HeLa cells (Bicego et al., 2006) and Sf9 cells (Oshima et al., 2003) demonstrate that, despite being correctly synthesized, targeted to the plasma membrane and the formation of normal gap junction plaques (Oshima et al., 2003), Cx26M34T gap junctions are functionally defective. Bicego et al. (2006) demonstrated that these gap junctions expressed in HeLa cells display an abnormal electrical behavior and a reduced unitary conductance (11%). Moreover, intercellular transfer of Lucifer yellow is prevented, and Cx26M34T channels fail to sustain the propagation of intercellular Ca^{2+} waves (Bicego et al., 2006). In the paired *Xenopus* oocyte system, homotypic Cx26M34T channels did not produce detectable currents, but when paired in a heterotypic combination with Cx26 wild-type, they showed altered gating with an inverted response to transjunctional voltage (Skerrett et al., 2004). In contrast, Oshima et al. (2003) showed, however that sulforhodamine dye transfer by GFP-tagged Cx26M34T is somewhat reduced, while the Cx26M34A mutant dye transfer is reduced by a factor of three to four.

To elucidate the pore-forming properties of Cx26 oligomers and gather information about the conductance states of Cx26 wild-type compared to Cx26M34A in a cell-free system, we made use of artificial planar membrane systems, which allow inserting Cx26 oligomers and monitoring their activity on a single channel level. Here, we used two different chip-based approaches for the electrophysiological characterization of the Cx26 isotypes. One is based on the application of giant unilamellar vesicles (GUVs) on an automated planar patch-clamp system. A single aperture produced in a borosilicate glass chip is employed, which has already greatly facilitated cell-based ion channel screening (Farre et al., 2007), single channel recordings in cell attached mode (Fertig et al., 2002a; Fertig et al., 2002b) and whole cell recordings (Fertig et al., 2002a, 2002b; Klemic et al., 2005; Sordel et al., 2006; Ionescu-Zanetti et al., 2005) by the possibility for automation and parallelization of the patch-clamp technique. The system has also been shown to be well suited for analyzing channel proteins reconstituted in artificial lipid membranes produced from fusion of GUVs (Schmidt et al., 2000; Sondermann et al., 2006). The second system is based on artificial planar lipid membranes formed on highly ordered mesoporous substrates, so-called nano-BLMs, which has been demonstrated to exhibit a very high long-term stability and allows monitoring channel activity of peptides and proteins

NIH-PA Author Manuscript

NIH-PA Author Manuscript

NIH-PA Author Manuscript

on a single channel level (Römer and Steinem, 2004; Römer et al., 2004; Pilz and Steinem, 2008). Schematics of the two membrane systems are displayed in Fig. 1.

2. Materials and methods

2.1. Materials

Aluminum substrates (thickness 0.5 mm, purity 99.999%) were purchased from Goodfellow (Huntington, UK). Tetradecanethiol (TDT), *n*-decane, *n*-octane, cholesterol, taurine, lanthanum, and sorbitol were obtained from Sigma-Aldrich (Taufkirchen, Germany). 1,2-Diphytanoyl-*sn*-glycero-3-phosphocholine (DPhPC) was purchased from Avanti Polar Lipids (Alabaster, AL, USA) and octyl-polyoxyethylene (o-POE) from Bachem (Bubendorf, Germany). Bio-Beads were obtained from Bio-Rad (Bio-Rad Laboratories GmbH, Munich, Germany).

2.2. Protein purification

Proteins were isolated from baculovirus-infected Sf9 cells according to published methods (Beahm et al., 2006; Oshima et al., 2003, 2007). In general, if hemichannels are stably expressed, protein preparations contain predominantly hexamers, but native gels also show a dodecameric band (Oshima and Fujiyoshi, unpublished observations). The human Cx26M34A Bac-N-Blue baculovirus construct (Invitrogen, Carlsbad, CA, USA) encoded a hexahistidine (His_6) tag with a thrombin cleavage site appended to the Cx26 *C*-terminus, while the pBlueBac (Invitrogen) rat Cx26 wild-type, which had a *C*-terminal thrombin cleavage site (LVPRGS), V5 epitope (GKPIPNPLLGLDST) and His_6 provided a significantly more efficient protein expression than a prior BacNBlue wild-type Cx26 construct (Oshima et al., 2003). Solubilized connexons were prepared from isolated Sf9 membranes by incubation in 2% dodecyl maltoside in HEPES buffer (10 mM HEPES, 1 M NaCl, 0.05% NaN_3, pH 7.5), and the proteins were purified using nickelnitrilotriacetic acid (Ni-NTA)-agarose beads. Samples were checked for purity by negatively staining with 2% uranyl acetate for electron microscopic observation and by Western blot and silver stain after electrophoresis on denaturing 4–20% gradient polyacrylamide gels (Invitrogen, Carlsbad, CA, USA).

2.3. Preparation of GUVs

Giant unilamellar vesicles (GUVs) composed of DPhPC/cholesterol (10:1) were prepared by the electroformation technique (Angelova and Dimitrov, 1986; Angelova and Dimitrov, 1988; Angelova, 2000) using two indium tin oxide (ITO) coated glass slides electrically connected to the Nanion Vesicle Prep Pro setup (Nanion Technologies GmbH, Munich, Germany). A DPhPC/cholesterol (10:1, 5 or 10 mM) mixture dissolved in chloroform was deposited on the ITO coated glass surface. After solvent evaporation, an O-ring was placed on the dried lipid film and 300 μl of a sorbitol solution (200 mM or 1 M) was carefully added to the lipid film. Then, the second ITO slide was placed on top of the O-ring with the ITO layer facing downwards. By application of an alternating electrical voltage of 3 V peak to peak for 2 h with a frequency of 5 Hz GUVs were formed, while keeping the temperature constant at 36 °C. Successful GUV formation was followed by analysis via an upright microscope.

2.4. Reconstitution of Cx26 in GUVs

Two approaches were followed to reconstitute Cx26 wild-type and its mutant Cx26M34A in GUVs:

i. For the procedure developed by Rigaud and colleagues (Rigaud and Levy, 2003; Girard et al., 2004), first proteoliposomes are formed, which are then transformed into GUVs. Briefly, DPhPC/cholesterol (10:1) dissolved in chloroform were dried at the bottom of glass tubes and resuspended in 2 mM TRIS/HCl, pH 7.0 followed by 2 h

NIH-PA Author Manuscript

NIH-PA Author Manuscript

NIH-PA Author Manuscript

of sonication to obtain a liposome suspension with a lipid concentration of 4 mg/ml. The liposomes were solubilized to form mixed micelles by addition of the detergent o-POE. Purified Cx26 (1 mg/ml) was added to the solution at a ratio of 1:500 and incubated for 30 min. Then, the detergent was removed by using Bio-beads twice for 2 h. After discarding the Bio-beads by centrifugation, the proteoliposomes (20 μl) were deposited on an ITO slide, partially dehydrated overnight and then subjected to the GUV formation procedure using 200 mM sorbitol.

ii. For the second procedure, first GUVs composed of DPhPC/cholesterol (10:1) were formed. Reconstitution of Cx26 was then achieved by incubating purified Cx26 dissolved in o-POE (lipid- to-protein ratio, 1:500) with preformed GUVs as described by Kreir et al. (2008). The detergent was removed at 4 °C by using Bio-beads overnight.

2.5. Formation of planar lipid bilayers on microstructured glass supports

Solvent-free planar lipid bilayers were formed in an automatic manner by bursting of GUVs after gentle suction through a micron-sized aperture (diameter of about 1–2 μm) in a borosilicate glass substrate using a Port-a-Patch setup (Nanion Technologies GmbH, Munich, Germany). To form planar lipid bilayers containing Cx26, 1–3 μl of protein-containing GUVs were pipetted onto the glass chip. GUVs are positioned onto the micron-sized aperture by applying a slightly negative pressure of −10 to −40 mbars. When a GUV touches the glass surface of the chip, it bursts and forms a planar bilayer (Sondermann et al., 2006) with a seal resistance of 10–100 GΩ.

2.6. Preparation and functionalization of porous alumina substrates

A detailed procedure of the preparation of porous alumina substrates is described elsewhere (Römer and Steinem, 2004). Briefly, aluminum foils were cleaned with ethanol, electropolished, and anodized in aqueous 0.3 M oxalic acid solution at $V = 40$ V and $T = 1.5$ °C for 5 days. To remove the underlying aluminum layer the porous alumina substrates were incubated with a saturated $HgCl_2$-solution. Pore bottoms were removed by chemical etching at $T = 30$ °C with 10 wt% phosphoric acid solution. The bottom surface was coated with 2.5 nm titanium and a 25 nm gold layer (Cressington sputter coater 108auto, Cressington MTM-20, Elektronen-Optik-Service, Dortmund, Germany), which was functionalized with tetradecanethiol (1 mM ethanolic solution, $t > 12$ h). After rinsing with ethanol, the hydrophobic substrate was vertically clamped in a Teflon cell, which was used for impedance analysis and single channel recordings.

2.7. Formation of nano-BLMs and reconstitution of Cx26

The *cis* and *trans* compartments of the Teflon cell were each filled with 1.5 ml electrolyte solution (10 mM HEPES, 200 mM KCl, 0.02 mM EDTA, pH 7.4). To prepare pore-suspending membranes (nano-BLMs), 2.5 μl of a solution of 20 mM DPhPC in *n*-decane/*n*-octane (1:1) was applied to the surface of the functionalized porous substrate. After impedance analysis of the formed nano-BLM, 0.5–2 μl of a 2 μg/ml Cx26 solution (1% *v*/*v* o-POE) was added to the *cis* side of the cell, leading to a final concentration of 0.7–2.7 ng/ml.

2.8. Impedance spectroscopy

The formation of nano-BLMs as well as their electrical characteristics were investigated by impedance analysis using the gain/phase analyzer SI 1260 and the 1296 Dielectric Interface (Solartron Instruments, Farnborough, UK) as described previously (Schmitt et al., 2008). Platinized platinum wires served as working and counter electrodes.

NIH-PA Author Manuscript

NIH-PA Author Manuscript

NIH-PA Author Manuscript

2.9. Single channel current recordings

Two different setups were used for single channel recordings:

- **i.** Recordings on bilayers spanning a single micron-sized hole in a glass substrate were performed with an automated patchclamp system, the Port-a-Patch (Nanion Technologies GmbH, Munich, Germany). Electrical recordings were performed with an EPC-10 patch-clamp amplifier (HEKA Electronics, Lambrecht/Pfalz, Germany) using the Patchmaster software (HEKA Electronics). Data were filtered at 3 kHz (Bessel filter) and digitized at a sampling rate of 50 kHz. Single channel data for analysis were filtered digitally at 1 kHz (Clampfit software, Axon Instruments, Sunnyvale, CA, USA).
- **ii.** Current recordings on nano-BLMs with membrane resistances of $>10^9$ Ω were obtained using an Axopatch 200B patchclamp amplifier (Axon Instruments) digitized at 10 kHz sampling rate. To avoid mechanical vibrations and interference from electric fields during the measurement, a Teflon cell equipped with two Ag/AgCl electrodes in the *cis* and *trans* compartment was placed in a Faraday cage on a mechanically isolated support. The electrode of the *trans* compartment was grounded and all potential differences are given relative to ground. The analog output signals were filtered with a low-pass four-pole Bessel filter at 1 kHz and digitized by an A/D converter (Digidata 1322, Axon Instruments). To control data recording and for analysis, the software package pClamp9.2 (Axon Instruments) was used. Prior to analysis, data were filtered with a 100 Hz low-pass Gaussian filter.

3. Results and discussion

3.1. Connexon preparation and analysis

By using the baculovirus-Sf9 system we were able to over-express rat Cx26WT-V5-His_6 and mutant human Cx26M34A-His_6. Rat and human Cx26WT-GFP-tetracysteine both express well in HeLa cells, however, rat Cx26WT tends to form larger gap junctions than human Cx26WT (data not shown) and therefore, we typically use rat Cx26WT. After purification by a nickel-NTA resin, samples were analyzed for concentration and purity. Assessments for purity were based on silver stained denaturating gels, in which the bands were identified as Cx26 species using Western blotting. In Fig. 2, the Cx26 band maps above the 22 kDa of the marker band, but it is visible also the dimer (~52 kDa), the trimer (~78 kDa) and the tetramer (~104 kDa). Extra bands can be explained by aggregation of Cx26 with proteolytic fragments of itself (for example the band above the 36 kDa should be 26 kDa + 13 kDa). These aggregates are commonly seen in SDS-PAGE. However, our electron microscopy and a native gel analysis of the same samples confirm a uniform channel appearance with only hexameric or dodecameric bands in Blue Native gels, indicating no oligomer heterogeneity in the preparations used in this particular set of experiments. It should also be noted that Western blotting accentuates minor bands seen in the silver stain protein gels because Western blotting is not a quantitative enzymatic technique.

3.2. Planar bilayers on microstructured glass chips

To carry out electrophysiological analysis of connexons, proteins were first reconstituted into GUVs. Subsequently, these proteoliposomes were pipetted onto a microstructured glass chip containing a single aperture with a size of a few micrometers. By suction application they were positioned and then fused onto the aperture in the glass chip resulting in a planar highly insulating lipid bilayer containing connexons with a membrane resistance in the GΩ regime (Fig. 1A).

NIH-PA Author Manuscript

NIH-PA Author Manuscript

NIH-PA Author Manuscript

3.3. Activity of Cx26 oligomers in planar bilayers on microstructured glass chips

Two different methods were used to reconstitute Cx26 into GUVs (see Section 2). Independent of the chosen method, the same protein activity was observed. Directly after the GΩ seal has been formed, activity of Cx26 wild-type oligomers can be monitored (Fig. 3). We were able to distinguish between three different conductance levels while varying the holding potential between −150 mV and +150 mV; G_1 = (38 ± 10) pS (n = 13, where n is the number of planar membrane preparations), G_2 = (101 ± 20) pS (n = 23) and G_3 = (156 ± 20) pS (n = 8). The conductance levels G_1 and G_2 both appear very frequently during the recordings, with G_1 being even more prominent at higher voltages of ±100 mV to ±150 mV. The conductance level G_3 was, however, less frequently observed. Fig. 3A/B depicts two characteristic current traces of Cx26 wild-type activity with conductance levels G_2 (Fig. 3A) and G_1 (Fig. 3B). The current-voltage relationship demonstrates the Ohmic behavior of the Cx26 oligomer (Fig. 3C and D). We determined the average conductance of the activity of Cx26 wild-type from several membrane preparations to (95 ± 2) pS (Fig. 3C) and (43 ± 2) pS (Fig. 3D). As Cx26 wild-type shows a broad distribution of conductances as reported in the literature (Falk et al., 1997;Buehler et al., 1995;Gonzalez et al., 2006), the mean conductance values were determined from single channel activity exhibiting one open level. Associated with the current generally observed for the hemichannel Cx26 wild-type, we also observed intermediate current signals suggesting subconductance states of the connexon (data not shown). Subconductance states were already described for other gap junctions, *e.g.*, Cx30 and Cx46 (Vogel et al., 2006;Trexler et al., 1996).

To elucidate the specificity of the observed connexon hemichannel activity, we investigated the influence of compounds known to inhibit the ion transport through Cx26 hemichannels. Several studies report on the effect of acidification-based closure of Cx26 hemichannels by protonated aminosulfonates (Tao and Harris, 2004; Yu et al., 2007; Bevans and Harris, 1999). In Fig. 4A/B, the effect of the addition of 50 mM taurine (pK_S (amine) = 8.74) at pH 7.0 on the activity of Cx26 wild-type is shown. Around 1 min after the addition of taurine, the conductance level is reduced from 89 pS to 16 pS. Fig. 4C/D shows the modulation of the activity of Cx26 wild-type upon addition of protonated HEPES (pK_S (amine) = 7.55). While characteristic hemichannel activity of Cx26 wild-type was monitored at pH 5.8 (10 mM TRIS/HCl, 200 mM KCl, 2 mM EDTA, pH 5.8) with a conductance of 82 pS, perfusion of HEPES buffer at pH 5.8 results in an immediate reduction of Cx26 activity (Bevans and Harris, 1999; Yu et al., 2007). Concentration dependent experiments reveal a complete loss of activity at 50 mM HEPES (50 mM HEPES, 200 mM KCl, 2 mM EDTA, pH 5.8).

Since it is known that the crystal structure of Cx26M34A shows a plug-like density at the cytoplasmic mouth of the pore (Oshima et al., 2007), we asked the question whether and how the mutation influences the single channel activity of the oligomer. Thus, we elucidated the electrical characteristics of the mutant Cx26M34A under the same conditions as Cx26 wild-type. Fig. 5A depicts a representative current trace obtained from a planar lipid bilayer containing Cx26 M34A at +80 mV. The point-amplitude histogram reveals a conductance of (75 ± 6) pS. The current-voltage relationship obtained from different membrane preparations (Fig. 5B) allowed us to determine the mean conductance of Cx26M34A to be (70.00 ± 0.01) pS (n = 23) from the slope of the linear I-V-plot. Less frequently, we observed smaller conductance values around 30 pS. Hemichannel activity of Cx43 has been shown to be blocked by lanthanum (Contreras et al., 2002; Ye et al., 2003; Kondo et al., 2000). In our studies, the addition of 0.2 mM La^{3+} results in the complete loss of activity almost immediately after its addition (Fig. 5C/D).

NIH-PA Author Manuscript

NIH-PA Author Manuscript

NIH-PA Author Manuscript

3.4. Nano-BLMs on ordered porous alumina

To investigate the influence of the membrane system on hemichannel activity, we compared and evaluated the results obtained for Cx26 wild-type and Cx26M34A in planar bilayers on micronsized apertures in glass with those obtained from nano-BLMs. In contrast to the planar bilayers on microstructured glass substrates, nano-BLMs are prepared from a lipid solution dissolved in an organic solvent and the protein is inserted *after* the bilayer preparation from a detergent solution. The formation of nano-BLMs was achieved by spreading DPhPC dissolved in *n*-decane/*n*-octane on functionalized highly ordered porous alumina substrates with a mean diameter of 60 nm. Details about the formation process and the electrical properties of nano-BLM are described elsewhere (Schmitt et al., 2006). Briefly, the thinning process was followed time resolved by impedance analysis at a constant frequency of 10^6 Hz. Upon thinning of the lipid-solvent droplet to form a bilayer, a continuous shift of the phase angle at 10^6 Hz from −85° to almost 0° is observed. Subsequently, an impedance spectra within a frequency range of 10^{-3}–10^6 Hz was taken and an equivalent circuit composed of a parallel *RC*-element (R_m = membrane resistance, C_m = membrane capacitance) representing the electrical behavior of a lipid bilayer in series to an Ohmic resistance R_{el} rep-resenting the electrolyte solution was fit to the data. Nano-BLMs with membrane resistances $R_m > 10^9$ Ω and a specific membrane capacitance C_m in the range of 0.2–0.5 μF/cm^2 were well suited for long-term, low noise single channel recordings.

3.5. Activity of Cx26 oligomers in nano-BLMs

Reconstitution of Cx26 oligomers into membranes was achieved by adding the protein in detergent solution to the *cis* compartment of the Teflon cell (see Fig. 1B). Since the insertion of a Cx26 oligomer was a random process, activity was observed sometimes already after several minutes but sometimes only after hours. If a hemichannel was inserted, current traces were recorded and different holding potentials ranging between +150 mV and −150 mV were applied. Fig. 6A shows a characteristic current trace of Cx26 wild-type after its insertion in a nano-BLM at a holding potential of +100 mV. Varying the holding potential between +150 mV and −150 mV and monitoring the current (Fig. 6B) demonstrates the Ohmic behavior of the hemichannel with a mean conductance of (33 ± 3) pS in agreement to our results obtained for Cx26 wild-type hemichannels inserted into planar bilayers on the microstructured glass support. Owing to the Ohmic behavior, we used all single channel events detected at different holding potentials for an event-histogram analysis. A statistical analysis of about 3000 events (Fig. 6C) reveals one prominent conductance state with a mean conductance of G_1 = (34 ± 8) pS. Less frequently, larger conductance states can be observed with two accumulations at G_2 = (70 ± 8) pS and G_3 = (165 ± 19) pS. The observed conductance distributions are in good accordance with those found for hemichannel activity in planar bilayers on the microstructured glass support. Other groups report on single channel conductance of reconstituted hemichannels in the range of 35–316 pS (Falk et al., 1997;Buehler et al., 1995;Gonzalez et al., 2006), while the single channel conductance of gap junctions of Cx26 wild-type is found to be in between 70 and 150 pS (Beltramello et al., 2005;Bicego et al., 2006;Gong and Nicholson, 2001;Suchyna et al., 1999;Kwak et al, 1995;Kojima et al., 1999).

We next investigated the activity of Cx26M34A reconstituted in nano-BLMs. We also found single channel activity after its reconstitution (Fig. 7A) with an Ohmic behavior in the voltage regime of −150 mV to +150 mV (Fig. 7B). The slope and hence the conductance of Cx26M34A hemichannels was calculated to be (53 ± 2) pS. The event-histogram of Cx26M34A hemichannel activity (about 4000 events) reveals only two, however rather defined main conductance states (Fig. 7C) with G_1 = (44 ± 6) pS being the most prominent one and G_2 = (69 ± 10) pS, which is more frequently observed than the second conductance state of the wild-type hemichannel. The fact that the mutant hemichannel is more frequently found in the conductance state G_2 compared to the wild-type is also reflected in the larger average

NIH-PA Author Manuscript

NIH-PA Author Manuscript

NIH-PA Author Manuscript

conductance determined from the slope of the *I-V*-characteristic (Fig. 7C). Larger conductances above 100 pS as observed for the wild-type were not found for the mutant in accordance with the current recordings obtained from hemichannels reconstituted in planar bilayers on a micro-sized glass support.

3.6. Comparison and overall discussion

In summary, we conclude that both systems presented in this study, solvent-free membranes on microstructured glass chips with already reconstituted Cx26 hemichannels and solvent-containing nano-BLMs, in which hemichannels were reconstituted afterwards, deliver the same results with respect to the main conductance levels of Cx26 wild-type and its mutant M34A. Of note, the mutant Cx26M34A also forms conductive hemichannels in these artificial membranes with two main conductance levels at around 40 and 70 pS. The specificity of the observed signals was proven in the planar membrane system on microstructured glass by the known acidification-based closure of Cx26 hemichannels by protonated aminosulfonates (Tao and Harris, 2004; Yu et al., 2007; Bevans and Harris, 1999). For the mutant Cx26M34A hemichannels, lanthanum was used as a blocking agent showing that 0.2 mM La^{3+} is sufficient to fully suppress the observed activity.

To date, channel recordings on Cx26 wild-type gap junctions were mainly performed by dual-whole-cell (paired cell system) experiments. The results reveal conductances in the range of 100–150 pS (Beltramello et al., 2005; Bicego et al., 2006; Gong et al., 2001; Suchyna et al., 1999; Kwak et al., 1995; Kojima et al., 1999; Oh et al., 1999; Mese et al., 2008). As the conductance of a hemichannel is twice the conductance of a gap junctional channel (Saez et al., 2005), the hemichannel conductance of Cx26 wild-type is expected to be in the range of 200–300 pS. In fact, channel recordings on single *Xenopus* oocytes in a cell attached configuration revealed a main open state conductance of (317 ± 12) pS (Gonzalez et al., 2006). In contrast to these findings, hemichannel conductance of purified or cell-free synthesized and subsequently reconstituted hemichannels in artificial bilayers exhibit conductance states in the range of 40–100 pS (Buehler et al., 1995; Falk et al., 1997) with the majority of events between 20 and 60 pS. These results are consistent with our statistical analysis of conductance events of Cx26 wild-type oligomers providing evidence for the reconstitution of functional hemichannels, independent of the membrane system. However, our results and those of others (Buehler et al., 1995; Falk et al., 1997) also suggest that the lateral interactions between neighboring channels in gap junction plaques or other cellular conditions (*e.g.*, connexin interacting proteins) play an important role for the channel conductance of connexons.

For Cx26M34A, two of the three conductance states have been found with a slightly altered frequency of the first and second conductance state. Interestingly, the overall range of conductance states is narrower for the mutant (0–100 pS) compared to the wild-type (0–200 pS). Electron crystallographic analysis revealed a plug-like density at the cytoplasmatic mouth of the pore of Cx26M34A (Oshima et al., 2007), which is drastically reduced in case of an *N*-terminal deletion mutant Cx26M34Adel2-7 (Oshima et al., 2008). Macroscopic measurements like dye-transfer experiments on Cx26 gap junctions showed a reduced transfer of dye in case of Cx26M34A compared to the wild-type and Cx26M34T (Oshima et al., 2003). Even though the dye transfer through Cx26M34T gap junctions is similar to that through wild-type gap junctions, Skerrett et al. (2004) found that homotypic Cx26M34T gap junctions do not induce intercellular coupling, while heterotypic paring with Cx26 wild-type reveals functional channels with gating properties significantly different from those of the wildtype. Recently, Heyman and Burt (2008) also demonstrated that dye transfer and electrical activity are independent processes for Cx43 channels in mammalian gap junctions. Moreover, in paired cell systems, the properties of gap junctions and not hemichannels are monitored and the overall

NIH-PA Author Manuscript

NIH-PA Author Manuscript

NIH-PA Author Manuscript

conductance is averaged over the entire gap junction plaque. Hence, on a molecular level, a reduced overall gap junctional conductance can be a result of a lower conductance level induced by partially closed Cx26M34A gap junctions, and by their reduced open probability, respectively. In cellular systems, also a decreased expression rate and a decreased hemichannel-hemichannel docking needs to be taken into account. In conclusion, on the hemichannel level our results suggest that the mutant Cx26M34A is active in itself allowing the passage of ions through the pore.

Acknowledgments

We acknowledge financial support from the European Union within the framework of the Marie Curie Training Network019335 “Translocation” and from the Bundesministerium für Bildung und Forschung (BMBF 13N9110 and 13N9111). Support was contributed by National Science Foundation grant MCB0543934 (GES), National Institutes of Health grants GM072881 (GES) and GM065937 (GES). Some of this work was conducted at the National Center for Microscopy and Imaging Research at San Diego, which is supported by National Institutes of Health Grant RR04050 awarded to Dr. Ellisman. Dr. Oshima is supported by Grants-in-Aid for Specially Promoted Research, Grant-in Aid for the Global Century Centers of Excellence, Kyoto University, Japan Science and Technology Agency, and the Japan New Energy and Industrial Technology Development Organization (awarded to Yoshinori Fujiyoshi).

References

Ahmad S, Chen S, Sun J, Lin X. Connexins 26 and 30 are co-assembled to form gap junctions in the cochlea of mice. Biochem. Biophys. Res. Commun 2003;307:362–368. [PubMed: 12859965]

Angelova MI, Dimitrov DS. Liposome electroformation. Farad. Discuss. Chem. Soc 1986;81:303–311.

Angelova MI, Dimitrov DS. A mechanism of liposome electroformation. Prog. Colloid Polym. Sci 1988;76:59–67.

Angelova, MI. Liposome electroformation. In: Luisi, PL.; Walde, P., editors. Giant Vesicles. John Wiley and Sons; Chichester, UK: 2000. p. 27-36.

Beahm DL, Oshima A, Gaietta GM, Hand GM, Smock AE, Zucker SN, Toloue MM, Chandrasekhar A, Nicholson BJ, Sosinsky GE. Mutation of a conserved threonine in the third transmembrane helix of alpha- and beta-connexins creates a dominant-negative closed gap junction channel. J. Biol. Chem 2006;281:7994–8009. [PubMed: 16407179]

Beltramello M, Piazza V, Bukauskas FF, Pozzan T, Mammano F. Impaired permeability to Ins(1,4,5)P3 in a mutant connexin underlies recessive hereditary deafness. Nat. Cell. Biol 2005;7:63–69. [PubMed: 15592461]

Bevans CG, Harris AL. Regulation of connexin channels by pH. Direct action of the protonated form of taurine and other aminosulfonates. J. Biol. Chem 1999;274:3711–3719. [PubMed: 9920923]

Bicego M, Beltramello M, Melchionda S, Carella M, Piazza V, Zelante L, Bukauskas FF, Arslan E, Cama E, Pantano S, Bruzzone R, D’Andrea P, Mammano F. Pathogenetic role of the deafness-related M34T mutation of Cx26. Hum. Mol. Genet 2006;15:2569–2587. [PubMed: 16849369]

Buehler LK, Stauffer KA, Gilula NB, Kumar NM. Single channel behavior of recombinant beta 2 gap junction connexons reconstituted into planar lipid bilayers. Biophys. J 1995;68:1767–1775. [PubMed: 7542035]

Contreras JE, Sanchez HA, Eugenin EA, Speidel D, Theis M, Willecke K, Bukauskas FF, Bennett MV, Saez JC. Metabolic inhibition induces opening of unopposed connexin 43 gap junction hemichannels and reduces gap junctional communication in cortical astrocytes in culture. Proc. Natl. Acad. Sci. USA 2002;99:495–500. [PubMed: 11756680]

Falk MM, Buehler LK, Kumar NM, Gilula NB. Cell-free synthesis and assembly of connexins into functional gap junction membrane channels. EMBO J 1997;16:2703–2716. [PubMed: 9184217]

Farre C, Stoelzle S, Haarmann C, George M, Bruggemann A, Fertig N. Automated ion channel screening: patch clamping made easy. Expert Opin. Ther. Targets 2007;11:557–565. [PubMed: 17373884]

Fertig N, Blick RH, Behrends JC. Whole cell patch clamp recording performed on a planar glass chip. Biophys. J 2002a;82:3056–3062. [PubMed: 12023228]

Fertig N, Klau M, George M, Blick RH, Behrends JC. Activity of single ion channel proteins detected with a planar microstructure. Appl. Phys. Lett 2002b;81:4865–4867.

NIH-PA Author Manuscript

NIH-PA Author Manuscript

NIH-PA Author Manuscript

Forge A, Becker D, Casalotti S, Edwards J, Marziano N, Nevill G. Gap junctions in the inner ear: comparison of distribution patterns in different vertebrates and assessment of connexin composition in mammals. J. Comp. Neurol 2003;467:207–231. [PubMed: 14595769]

Gerido DA, White TW. Connexin disorders of the ear, skin, and lens. Biochim. Biophys. Acta 2004;1662:159–170. [PubMed: 15033586]

Girard P, Pecreaux J, Lenoir G, Falson P, Rigaud JL, Bassereau P. A new method for the reconstitution of membrane proteins into giant unilamellar vesicles. Biophys. J 2004;87:419–429. [PubMed: 15240476]

Gong XQ, Nicholson BJ. Size selectivity between gap junction channels composed of different connexins. Cell Commun. Adhes 2001;8:187–192. [PubMed: 12064586]

Gonzalez D, Gomez-Hernandez JM, Barrio LC. Species specificity of mammalian connexin-26 to form open voltage-gated hemichannels. FASEB J 2006;20:2329–2338. [PubMed: 17077310]

Harris AL. Emerging issues of connexin channels: biophysics fills the gap. Q Rev. Biophys 2001;34:325–472. [PubMed: 11838236]

Heyman N, Burt J. Hindered diffusion through an aqueous pore describes invariant dye selectivity of Cx43 junctions. Biophys. J 2008;94:840–854. [PubMed: 17921206]

Ionescu-Zanetti C, Shaw RM, Seo J, Jan YN, Jan LY, Lee LP. Mammalian electrophysiology on a microfluidic platform. Proc. Natl. Acad. Sci. USA 2005;102:9112–9117. [PubMed: 15967996]

Jentsch TJ. Neuronal KCNQ potassium channels: physiology and role in disease. Nat. Rev. Neurosci 2000;1:21–30. [PubMed: 11252765]

Kelsell DP, Dunlop J, Stevens HP, Lench NJ, Liang JN, Parry G, Mueller RF, Leigh IM. Connexin 26 mutations in hereditary non-syndromic sensorineural deafness. Nature 1997;387:80–83. [PubMed: 9139825]

Kikuchi T, Adams JC, Miyabe Y, So E, Kobayashi T. Potassium ion recycling pathway via gap junction systems in the mammalian cochlea and its interruption in hereditary nonsyndromic deafness. Med. Electron. Microsc 2000;33:51–56. [PubMed: 11810458]

Kikuchi T, Kimura RS, Paul DL, Adams JC. Gap junctions in the rat cochlea: immunohistochemical and ultrastructural analysis. Anat. Embryol 1995;191:101–118. [PubMed: 7726389]

Klemic KG, Klemic JF, Sigworth FJ. An air-molding technique for fabricating PDMS planar patch-clamp electrodes. Pflügers Arch 2005;449:564–572.

Kojima T, Srinivas M, Fort A, Hopperstad M, Urban M, Hertzberg EL, Mochizuki Y, Spray DC. TPA induced expression and function of human connexin 26 by post-translational mechanisms in stably transfected neuroblastoma cells. Cell Struct. Funct 1999;24:435–441. [PubMed: 10698257]

Kondo RP, Wang SY, John SA, Weiss JN, Goldhaber JI. Metabolic inhibition activates a non-selective current through connexin hemichannels in isolated ventricular myocytes. J. Mol. Cell. Cardiol 2000;32:1859–1872. [PubMed: 11013130]

Kreir M, Farre C, Beckler M, George M, Fertig N. Rapid screening of membrane protein activity: electrophysiological analysis of OmpF reconstituted in proteoliposomes. Lab Chip 2008;8:587–595. [PubMed: 18369514]

Kwak BR, Hermans MM, De Jonge HR, Lohmann SM, Jongsma HJ, Chanson M. Differential regulation of distinct types of gap junction channels by similar phosphorylating conditions. Mol. Biol. Cell 1995;6:1707–1719. [PubMed: 8590800]

Kyle JW, Minogue PJ, Thomas BC, Domowicz DA, Berthoud VM, Hanck DA, Beyer EC. An intact connexin N-terminus is required for function but not gap junction formation. J. Cell Sci 2008;121:2744–2750. [PubMed: 18664489]

Lautermann J, Frank HG, Jahnke K, Traub O, Winterhager E. Developmental expression patterns of connexin26 and −30 in the rat cochlea. Dev. Genet 1999;25:306–311. [PubMed: 10570462]

Mese G, Valiunas V, Brink P, White TW. Connexin26 deafness associated mutations show altered permeability to large cationic molecules. Am. J. Physiol. Cell Physiol 2008;295:C966–C974. [PubMed: 18684989]

Oh S, Rubin JB, Bennett MV, Verselis VK, Bargiello TA. Molecular determinants of electrical rectification of single channel conductance in gap junctions formed by connexins 26 and 32. J. Gen. Physiol 1999;114:339–364. [PubMed: 10469726]

NIH-PA Author Manuscript

NIH-PA Author Manuscript

NIH-PA Author Manuscript

Oh S, Abrams CK, Verselis VK, Bargiello TA. Stoichiometry of transjunctional voltage-gating polarity reversal by a negative charge substitution in the amino terminus of a connexin32 chimera. J. Gen. Physiol 2000;116:13–31. [PubMed: 10871637]

Oshima A, Doi T, Mitsuoka K, Maeda S, Fujiyoshi Y. Roles of Met-34, Cys-64, and Arg-75 in the assembly of human connexin 26, Implication for key amino acid residues for channel formation and function. J. Biol. Chem 2003;278:1807–1816. [PubMed: 12384501]

Oshima A, Tani K, Hiroaki Y, Fujiyoshi Y, Sosinsky GE. Three-dimensional structure of a human connexin26 gap junction channel reveals a plug in the vestibule. Proc. Natl. Acad. Sci. USA 2007;104:10034–10039. [PubMed: 17551008]

Oshima A, Tani K, Hiroaki Y, Fujiyoshi Y, Sosinsky GE. Projection structure of a N-terminal deletion mutant of connexin 26 channel with decreased central pore density. Cell Commun. Adhes 2008;15:85–93. [PubMed: 18649181]

Pilz C, Steinem C. Modulation of the conductance of a 2,2-bipyridine-functionalized peptidic ion channel by Ni^{2+} Eur. Biophys. J 2008;37:1065–1071. [PubMed: 18347789]

Purnick PE, Benjamin DC, Verselis VK, Bargiello TA, Dowd TL. Structure of the amino terminus of a gap junction protein. Arch. Biochem. Biophys 2000;381:181–190. [PubMed: 11032405]

Rigaud JL, Levy D. Reconstitution of membrane proteins into liposomes. Methods Enzymol 2003;372:65–86. [PubMed: 14610807]

Römer W, Steinem C. Impedance analysis and single-channel recordings on nano-black lipid membranes based on porous alumina. Biophys. J 2004;86:955–965. [PubMed: 14747331]

Römer W, Lam YH, Fischer D, Watts A, Fischer WB, Göring P, Wehrspohn RB, Gösele U, Steinem C. Channel activity of a viral transmembrane peptide in micro-BLMs: $Vpu_{1–32}$ from HIV-1. J. Am. Chem. Soc 2004;126:16267–16274. [PubMed: 15584764]

Saez JC, Retamal MA, Basilio D, Bukauskas FF, Bennett MV. Connexin-based gap junction hemichannels: gating mechanisms. Biochim. Biophys. Acta 2005;1711:215–224. [PubMed: 15955306]

Schmidt C, Mayer M, Vogel H. A chip-based biosensor for the functional analysis of single ion channels. Angew. Chem. Int. Ed 2000;39:3137–3140.

Schmitt EK, Nurnabi M, Bushby RJ, Steinem C. Electrically insulating pore-suspending membranes on highly ordered porous alumina obtained from vesicle spreading. Soft Matter 2008;4:250–253.

Schmitt EK, Vrouenraets M, Steinem C. Channel activity of OmpF monitored in nano-BLMs. Biophys. J 2006;91:2163–2171. [PubMed: 16782785]

Skerrett IM, Di WL, Kasperek EM, Kelsell DP, Nicholson BJ. Aberrant gating, but a normal expression pattern, underlies the recessive phenotype of the deafness mutant connexin26M34T. FASEB J 2004;18:860–862. [PubMed: 15033936]

Sondermann M, George M, Fertig N, Behrends JC. High-resolution electrophysiology on a chip: transient dynamics of alamethicin channel formation. Biochim. Biophys. Acta 2006;1758:545–551. [PubMed: 16696935]

Sordel T, Garnier-Raveaud S, Sauter F, Pudda C, Marcel F, De Waard M, Arnoult C, Vivaudou M, Chatelain F, Picollet-D'hahan N. Hourglass SiO_2 coating increases the performance of planar patch-clamp. J. Biotechnol 2006;125:142–154. [PubMed: 16595156]

Suchyna TM, Nitsche JM, Chilton M, Harris AL, Veenstra RD, Nicholson BJ. Different ionic selectivities for connexins 26 and 32 produce rectifying gap junction channels. Biophys. J 1999;77:2968–2987. [PubMed: 10585920]

Tao L, Harris AL. Biochemical requirements for inhibition of connexin26-containing channels by natural and synthetic taurine analogs. J. Biol. Chem 2004;279:38544–38554. [PubMed: 15234974]

Trexler EB, Bennett MV, Bargiello TA, Verselis VK. Voltage gating and permeation in a gap junction hemichannel. Proc. Natl. Acad. Sci. USA 1996;93:5836–5841. [PubMed: 8650179]

Vogel R, Valiunas V, Weingart R. Subconductance states of Cx30 gap junction channels: data from transfected HeLa cells versus data from a mathematical model. Biophys. J 2006;91:2337–2348. [PubMed: 16782793]

Ye ZC, Wyeth MS, Baltan-Tekkok S, Ransom BR. Functional hemichannels in astrocytes: a novel mechanism of glutamate release. J. Neurosci 2003;23:3588–3596. [PubMed: 12736329]

NIH-PA Author Manuscript

NIH-PA Author Manuscript

NIH-PA Author Manuscript

Yu J, Bippes CA, Hand GM, Muller DJ, Sosinsky GE. Aminosulfonate modulated pH-induced conformational changes in connexin26 hemichannels. J. Biol. Chem 2007;282:8895–8904. [PubMed: 17227765]

Zhang Y, Tang W, Ahmad S, Sipp JA, Chen P, Lin X. Gap junction-mediated intercellular biochemical coupling in cochlear supporting cells is required for normal cochlear functions. Proc. Natl. Acad. Sci. USA 2005;102:201–206.

NIH-PA Author Manuscript
NIH-PA Author Manuscript
NIH-PA Author Manuscript

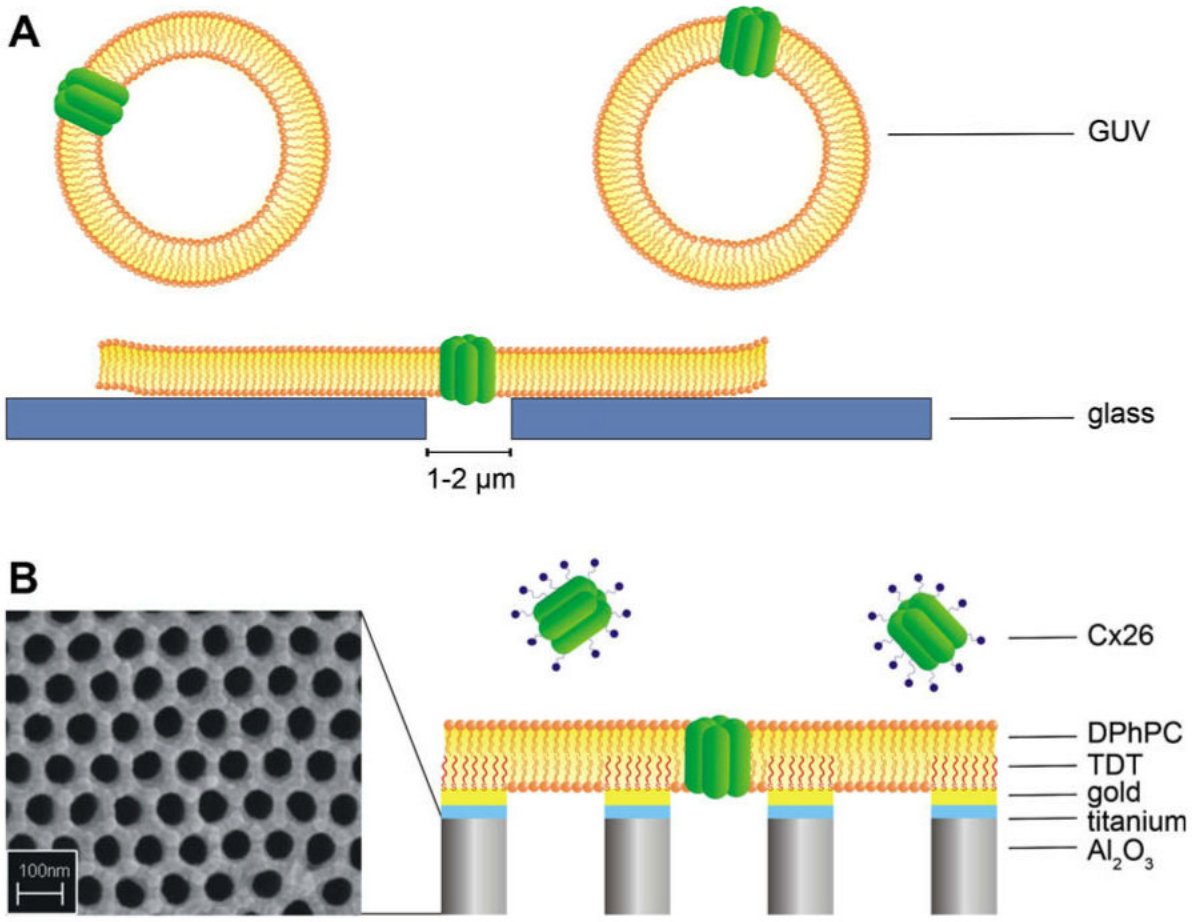

Fig. 1.

Schematic illustration (not drawn to scale) of the two setups used in this study. (A) Formation of planar lipid bilayers on microstructured glass supports by gentle suction of Cx26 containing giant unilamellar vesicles (GUVs). (B) Detergent-based reconstitution of Cx26 into nano-BLMs. The nanostructured porous alumina is coated with a thin layer of titanium and gold. After functionalizing the gold surface with tetradecanethiol (TDT) the pore-suspending bilayer is generated by applying 1,2-diphytanoyl-*sn*-glycero-3-phosphocholine (DPhPC) dissolved in *n*-decane/*n*-octane (1:1) to the surface.

NIH-PA Author Manuscript
NIH-PA Author Manuscript
NIH-PA Author Manuscript

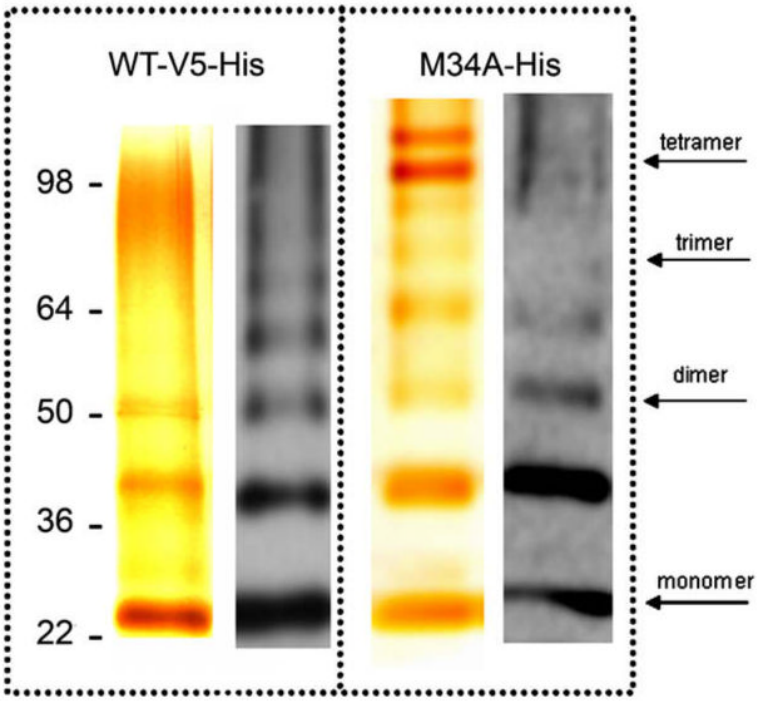

Fig. 2.

Protein purification. Cx26WT and Cx26M34A mutant analysis by silver staining (left) and Western blot (right). The WT shows clearly two bands, corresponding to the monomer, dimer and possibly the tetramer mapping around 104 kDa of the marker band. The extra band above 36 kDa may be explained with oligomerization of Cx26 with a truncated form of itself. The Western blot detects the same bands, plus other oligomers, suggesting that the preparation consists almost entirely of Cx26. The Cx26M34A shows also a trimeric form above the 64 kDa band. Oligomeric bands are typically an aggregation product that occurs during the sample preparation for SDS-PAGE.

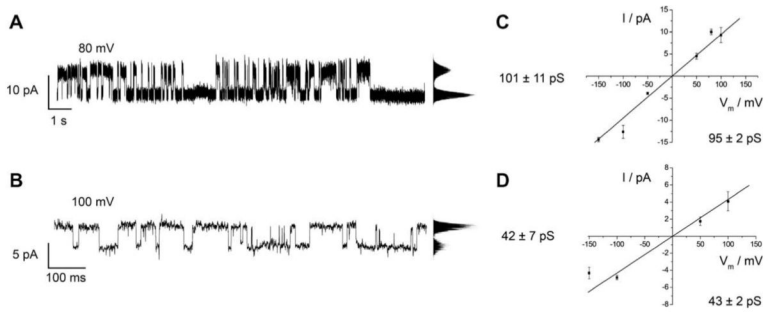

Fig. 3.

Single channel recordings on Cx26 wild-type oligomers inserted in a planar lipid bilayer on a micron-sized aperture in glass. (A/B) Characteristic current traces of Cx26 wild-type obtained at +100 mV in 10 mM HEPES, 200 mM KCl, 2 mM EDTA, pH 7.0. The point-amplitude histogram reveals a conductance of (101 ± 11) pS (A) and (42 ± 7) pS (B). (C/D) Cx26 wild-type current-voltage relationships. The main conductance was calculated from the slope of the linear regression and was determined to be (95 ± 2) pS (C) and (43 ± 2) pS (D).

NIH-PA Author Manuscript NIH-PA Author Manuscript NIH-PA Author Manuscript

NIH-PA Author Manuscript

NIH-PA Author Manuscript

NIH-PA Author Manuscript

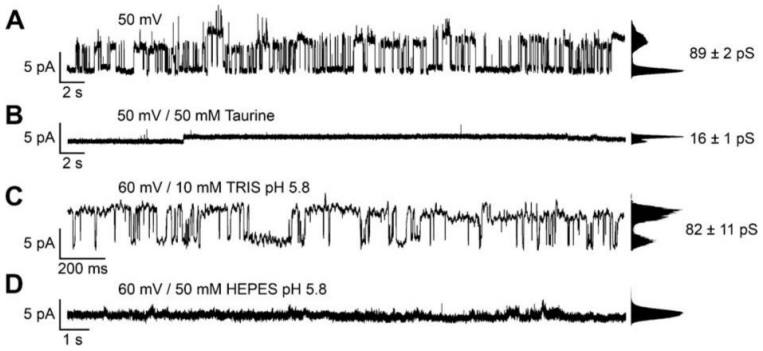

Fig. 4.

Modulation of Cx26 wild-type activity inserted in a planar lipid bilayer on a micron-sized aperture in glass by protonated taurine and HEPES. (A) Current trace of Cx26 wild-type oligomers obtained at +50 mV in 10 mM HEPES, 200 mM KCl, 2 mM EDTA, pH 7.0. The point-amplitude histogram reveals a conductance of (89 ± 2) pS. (B) Current trace around 1 min after the addition of 50 mM taurine. (C) Current trace of Cx26 wild-type obtained at +60 mV in 10 mM TRIS/HCl, 200 mM KCl, 2 mM EDTA, pH 5.8 The point-amplitude histogram reveals a conductance of (82 ± 11) pS. (D) Single channel recordings about 1 min after the addition of 50 mM HEPES.

NIH-PA Author Manuscript
NIH-PA Author Manuscript
NIH-PA Author Manuscript

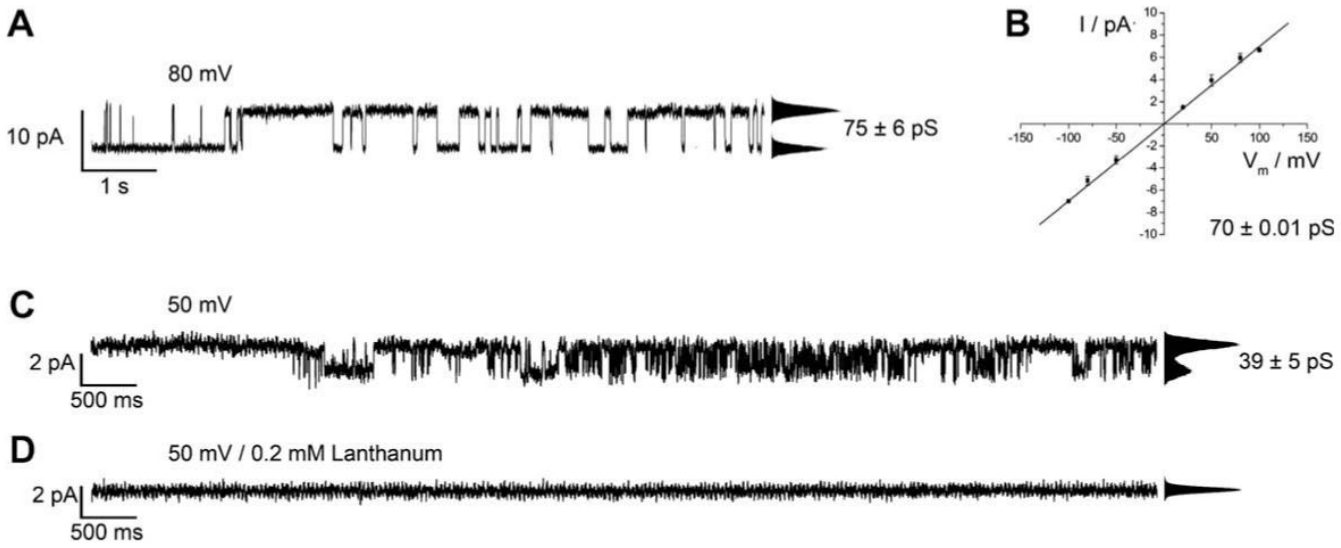

Fig. 5.

Single channel recordings of Cx26M34A inserted in a planar lipid bilayer on a micron-sized aperture in glass. (A) Representative current trace obtained from a planar bilayer containing Cx26M34A at +80 mV in 10 mM HEPES, 200 mM KCl, 2 mM EDTA, pH 7.0. The point-amplitude histogram reveals a conductance of (75 ± 6) pS. (B) Cx26M34A current-voltage relationship obtained by averaging the current amplitudes from several membrane preparations. The main conductance was obtained as the slope of the linear regression and was determined to be (70.00 ± 0.01) pS. (C) Current trace of Cx26M34A obtained at +50 mV in 10 mM HEPES, 200 mM KCl, 2 mM EDTA, pH 7.0. The point-amplitude histogram shows a conductance of (39 ± 5) pS. (D) Current trace monitored 1 min after the addition of 0.2 mM La^{3+}.

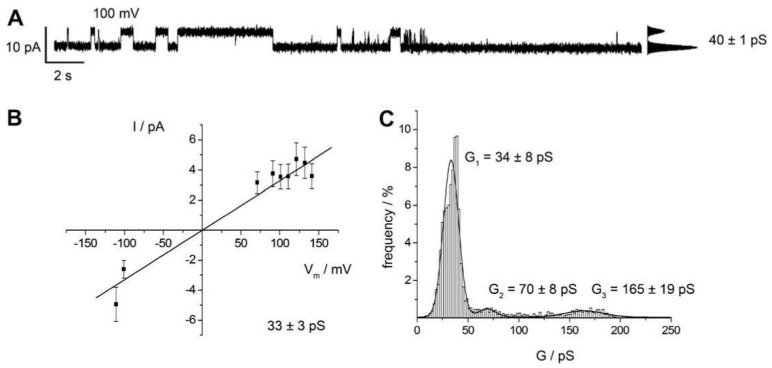

Fig. 6.

Single channel recordings of Cx26 wild-type in nano-BLMs. (A) Characteristic current trace of Cx26 wild-type obtained at +100 mV in 10 mM HEPES, 200 mM KCl, 0.02 mM EDTA, pH 7.4. The point-amplitude histogram reveals a conductance of (40 ± 1) pS. (B) Cx26 wild-type current-voltage relationship of averaged current steps ranging between 0 and 63 pS [2169 events]. The hemichannel shows a linear *I-V*-dependence with a main conductance of (33 ± 3) pS. (C) Event-histogram of the observed conductance states of Cx26 wild-type in nano-BLMs [2691 events, bin width: 2 pS]. The solid lines are the results of fitting three Gaussian distributions to the histogram. Three main conductance states are assigned with G_1 = (34 ± 8) pS, G_2 = (70 ± 8) pS and G_3 = (165 ± 19) pS.

NIH-PA Author Manuscript NIH-PA Author Manuscript NIH-PA Author Manuscript

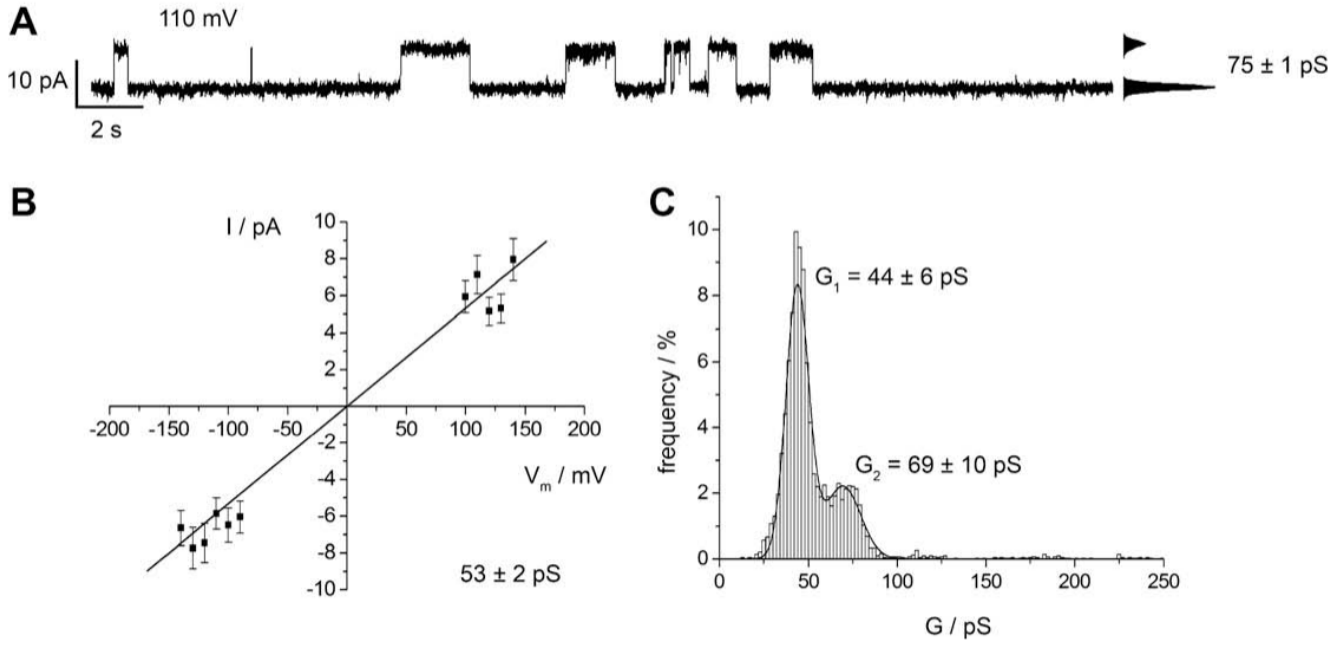

Fig. 7.

Single channel recordings of Cx26M34A oligomers in nano-BLMs. (A) Characteristic current trace of Cx26M34A obtained at +110 mV in 10 mM HEPES, 200 mM KCl, 0.02 mM EDTA, pH 7.4. The point-amplitude histogram reveals a conductance of (75 ± 1) pS. (B) Cx26 M34A current-voltage relationship of averaged current steps ranging between 0 and 70 pS [3476 events]. The hemichannel shows a linear *I-V*-dependence with a main conductance of (53 ± 2) pS. (C) Event-histogram analysis of the observed conductance states of Cx26 M34A in nano-BLMs [4137 events, bin width: 2 pS]. The solid lines are the results of fitting two Gaussian distributions to the histogram. Two main conductance states are assigned with G_1 = (44 ± 6) pS and G_2 = (69 ± 10) pS.

NIH-PA Author Manuscript NIH-PA Author Manuscript NIH-PA Author Manuscript